AGU PUBLICATIONS

JGR

Journal of Geophysical Research: Oceans

RESEARCH ARTICLE

10.1002/2013JC009118

Key Points:
- Report evidence of a inertially generated coastal-trapped waves
- Study the process that triggers coastal-trapped waves in the tropical Pacific
- High-frequency radars and its ability of detecting complex ocean features

Correspondence to:
X. Flores-Vidal,
floresx@uabc.edu.mx

Citation:
Flores-Vidal, X., R. Durazo, L. Zavala-Sansón, P. Flament, C. Chavanne, F. J. Ocampo-Torres, and C. Reyes-Hernández (2014), Evidence of inertially generated coastal-trapped waves in the eastern tropical Pacific, *J. Geophys. Res. Oceans*, *119*, 3121–3133, doi:10.1002/2013JC009118.

Received 16 MAY 2013
Accepted 28 APR 2014
Accepted article online 3 MAY 2014
Published online 29 MAY 2014

Evidence of inertially generated coastal-trapped waves in the eastern tropical Pacific

X. Flores-Vidal[1], R. Durazo[2], L. Zavala-Sansón[3], P. Flament[4], C. Chavanne[5], F. J. Ocampo-Torres[3], and C. Reyes-Hernández[6]

[1]Instituto de Investigaciones Oceanológicas, Universidad Autónoma de Baja California, Ensenada, Baja California, Mexico, [2]Facultad de Ciencias Marinas, Universidad Autónoma de Baja California, Ensenada, Baja California, Mexico, [3]Departamento de Oceanografía Física, Centro de Investigación Científica y de Educación Superior de Ensenada, Ensenada, Baja California, Mexico, [4]Department of Oceanography, School of Ocean and Earth Science and Technology, University of Hawaii at Manoa, Honolulu, Hawaii, USA, [5]Institut des Sciences de la Mer de Rimouski, Université du Québec à Rimouski, Rimouski, Québec, Canada, [6]Instituto de Recursos, Universidad Del Mar, Puerto Ángel, Oaxaca, Mexico

Abstract Observations of coastal-trapped waves (CTW) are limited by instrumentation technologies and temporal and spatial resolutions; hence, their complete description is still limited. In the present work, we used measurements from high-frequency radio scatterometers (HFR) to analyze the subinertial dynamics of the Gulf of Tehuantepec in the Mexican Pacific, a region strongly influenced by offshore gap winds. The data showed subinertial oscillations that may be explained by poleward propagating CTWs. The oscillations showed higher coherence (95% confidence) with gap winds in the Gulfs of Papagayo and Panama than with local winds. Vertical thermocline oscillations, measured with a moored thermistor-chain, also showed subinertial oscillations coherent with Papagayo and Panama winds. The period of the observed oscillations was ∼4 days, which corresponds to the inertial period of the Gulf of Panama. This suggests that inertial oscillations generated by offshore wind outbursts over Panama may have traveled northward along the coastal shelf, and were detected as surface current pulses by the HFR installed approximately 2000 km further north in the Gulf of Tehuantepec. To further explore the presence of CTWs, the 4 day band-pass filtered currents measured by the HFR were analyzed using empirical orthogonal functions. We found that the first mode behaved like a CTW confined to the shelf break. Additionally, the observed oscillations were compared with baroclinic and barotropic CTW models. The results support the notion that nearly inertial baroclinic CTWs are generated in the Gulfs of Panama and Papagayo and then propagate toward the Gulf of Tehuantepec.

1. Introduction

The coastal shelf break and the alongshore wind component are the main factors generating oceanic perturbations or waves that propagate along the left (right) side of the shelf in the northern (southern) hemisphere [*Clarke*, 1977; *Csanady*, 1977; *Brink*, 1982, 1991]. These waves are referred to as shelf waves, coastal-trapped waves (CTW), or hybrid waves, due to their shared characteristics with baroclinic Kelvin waves and barotropic shelf waves [*Mysak*, 1968; *Gill and Clarke*, 1974]. There are many theoretical and observational CTW studies [e.g., *Allen*, 1975; *Huthnance*, 1978; *Brink*, 1991] and is well known that in coastal zones CTWs provide an important input to subinertial motions from low (∼0–10°N) to high (∼20–30°N) latitudes [*Merrifield*, 1992; *Zamudio et al*., 2008].

The region of the eastern tropical Pacific Ocean, between the Gulf of Panama (∼7°N) and the Gulf of Tehuantepec (∼16°N) is characterized by the presence of geostrophic eddies generated mainly by strong wind jets that blow from the Atlantic to the Pacific through three main mountain gaps [*Brandhors*, 1958; *Blackburn*, 1962; *Steenburgh et al*., 1998; *Romero-Centeno et al*., 2003]. Nevertheless, the ocean's variability in the region is not only determined by gap winds but also by alongshore fronts [*Barton et al*., 2009]. Although linear CTWs imply no net transport, they may influence shelf processes, such as alongshore fronts and subinertial variability. However, spatial resolution of satellite products (i.e., altimetry) is too coarse to observe CTWs, and although sea level records along the Mexican Pacific shelf demonstrate their presence and propagation for approximately 2000 km along the coastline [*Merrifield*, 1992; *Christensen et al*., 1983; *Enfield and Allen*, 1983], studies to understand better the CTWs dynamics are still required. Furthermore, numerical

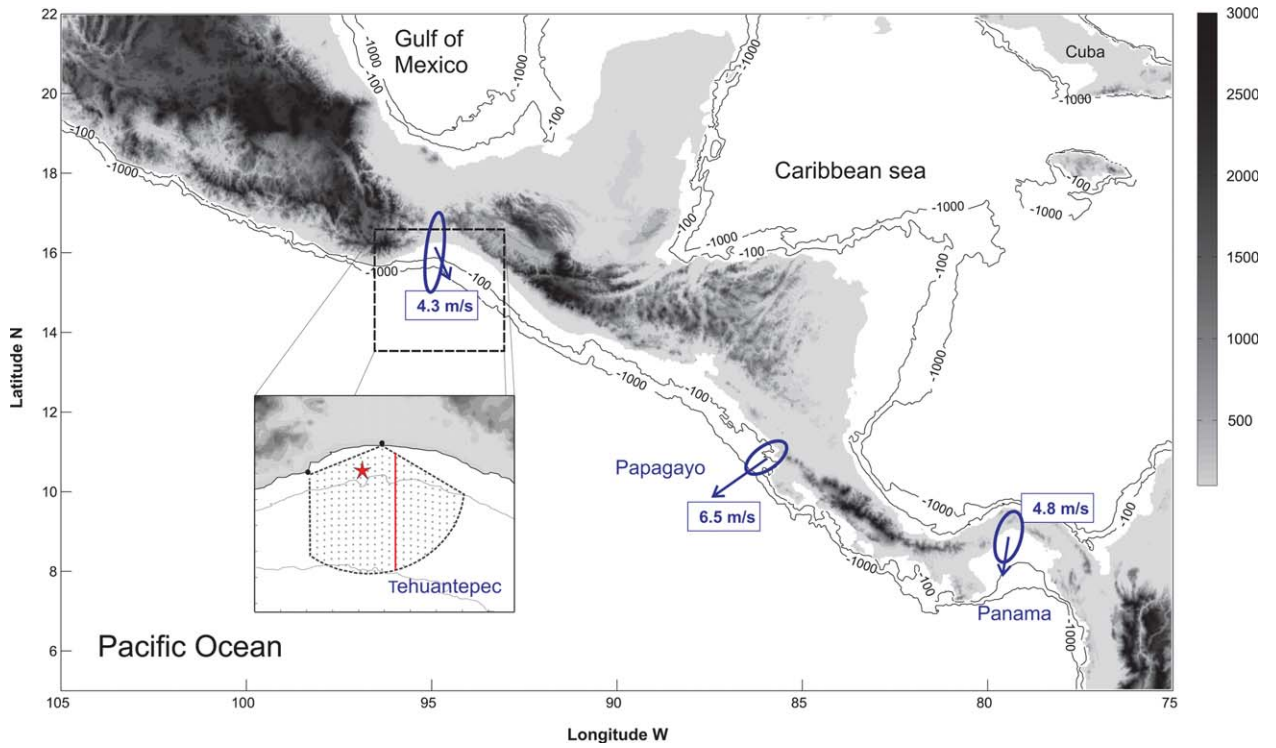

Figure 1. The study site southwest of Mexico and Central America. Mountain chains are represented by gray contours (positive elevations above mean sea level). The continental shelf is illustrated by the 100 and 1000 m isobaths. The location of the Gulfs of Tehuantepec, Papagayo, and Panama are indicated by wind variability ellipses and their mean vectors composed of 60 day time series. A zoom over the HFR footprint is shown: gray dots are the data over a Cartesian grid (dx,dy = 5 km), the red star shows the position of the mooring, the red line shows the cross-shore transect plotted in Figure 3.

simulations predict that CTWs on the Mexican Pacific shelf are originated at the Gulf of Panama and travel poleward up to Cabo Corrientes (∼20°N) without being affected by the wind jets over the Gulf of Papagayo (∼11°N) or Tehuantepec [*Zamudio et al*., 2001, 2006, 2008]. To our knowledge, there are no other studies, besides the ones mentioned here, that report or propose the presence of CTWs on the eastern tropical Pacific or at the Gulf of Tehuantepec in particular.

In the present work, we studied the subinertial variability of the Gulf of Tehuantepec using high-frequency Doppler radio scatterometers with high temporal and spatial resolutions which covered the coastal zone from ∼5 km to ∼100 km offshore, along with a moored acoustic Doppler current profiler (ADCP), thermistor-chain, satellite measurements of sea surface temperature (SST), and typical conductivity-temperature-depth (CTD) casts. The study was partially motivated by the recent reports of *Barton et al*. [2009] and *Flores-Vidal et al*. [2011], who have shown the presence of a warm, poleward flowing coastal front in the Gulf of Tehuantepec.

In the following section, we describe all the data used in this work. Section 3 shows the full set of observational results, based on which we studied the subinertial variability along the Mexican Pacific shelf. In section 4, we discuss our findings and propose CTWs as the physical mechanism that may explain part of the subinertial variability in the region. Finally, we make a few conclusions and suggest further research lines.

2. Data

The present work is based on data from two HF Doppler radio (HFR) scatterometers, which were deployed in the Gulf of Tehuantepec (GT) from 1 February 2008 to 31 March 2008. HFRs measured sea surface currents at hourly intervals with accuracy of ∼2.5 cm s^{-1}, mapping the coastal zone from ∼5 km to ∼100 km offshore with spatial resolution of 5 km (Figure 1). For a more detailed description of these measurements and HFR data in general, we refer to *Barrick* [1977], *Gurgel* [1999], and *Flores-Vidal et al*. [2011, 2013].

Additionally, a thermistor array mooring was installed inside the HFR footprint (~16°N, 95°W), approximately 20 km offshore (Figure 1). The mooring was also instrumented with a 600 kHz, downward-looking ADCP, which recorded current profiles of 2 m bins at hourly intervals from 10 to 40 m depth.

The measurements were complemented with satellite SST data from the *Physical Oceanography Distributed Active Archive Center* (PODAAC) (see http://podaac.jpl.nasa.gov) with spatial and temporal resolutions of 1/16° and 1 h, respectively, and with wind measurements from the *Cross-Calibrated Multi-Platform* (CCMP) (see http://apdrc.soest.hawaii.edu/datadoc/ccmp.php) with spatial and temporal resolutions of 1/4° and 6 h, respectively. Additionally, we made use of CTD profiles obtained during a 5 day cruise carried out in summer 2008. The CTD profiles were not taken simultaneously with the other measurements, but its geostrophic nature recorded in the absence of wind jets is therefore very illustrative for the purposes of the present study.

Unless stated otherwise, all the data presented here were low-pass filtered using a Lanczos filter with a cutoff period of 72 h. Spectral and coherence analyses [*Gonella*, 1972; *Fofonoff*, 1969] were performed using data sampled at an hourly rate, except for the CCMP wind analysis, which was based on data sampled at a rate of 6 h. The length of the time series (60 days) allowed us to make spectral partitions of 10 days, yielding spectral partitions of $N = 240$ points and a Nyquist frequency of 12 cycles per day (cpd). For the wind records, these values were $N = 40$ and a Nyquist frequency of 2 cpd. Finally, a Blackman-Harris window to reduce sidelobe leakage was applied to each partition. For each case, the 95% confidence interval was estimated.

3. Results

Eastern tropical Pacific gap wind variability is influenced by three orographic steps: the Gulf of Tehuantepec (GT), the Gulf of Papagayo (GPP), and the Gulf of Panama (GPN). Component ellipses and mean vectors for each of the three locations are shown in Figure 1. Ellipse axes and mean vectors were computed using February 2008 and March 2008 CCMP wind records, based on the spatial average of the four grid cells closest to the coast of each location. In the GT, the orographic depression influenced the wind jet almost entirely on the cross-shore component. The relatively small mean vector compared to the variability suggests that wind jets were common but not permanent. By contrast, the mean vectors in the GPN and, more notably, in the GPP were larger than their corresponding variability. This suggests that the wind jets over the GPN and the GPP were stronger and almost permanent. Mean wind jet speed in the GPP was 6.5 ms^{-1}, while in the GT and the GPN, it was 4.3 ms^{-1} and 4.8 ms^{-1}, respectively. The rotary power spectra, obtained before applying the low-pass filter to the wind time series, showed a diurnal peak at the three locations, and a semidiurnal peak only in the GPP (Figure 2a). On the lower frequency domain, inertial peaks were found with periods of 1.8 days in the GT (16°N), 2.6 days in the GPP (11°N), and 4 days in the GPN (7°N).

The rotary power spectrum of sea surface currents was obtained from the spatial average of the HFR grid, before applying the low-pass filter (Figure 2b). The four main peaks in the spectrum indicate a semidiurnal, diurnal, inertial, and half the inertial frequency (twice the period). Anticyclonic rotation was observed for inertial and semidiurnal peaks, and cyclonic for the subinertial peak located between 3 and 5 days. This subinertial variability is the focus of the present work.

The subinertial temporal and spatial variability of the sea surface currents along one cross-shore transect (red line in Figure 1) is shown in Figure 3. When the wind stress magnitude was above the absolute threshold value, SST decreased ~10°C, the mean westward flow veered to the south, and the thermocline was pumped up to the surface from an average depth of ~30 m (e.g., on 28 February 2008). By contrast, throughout the entire studied period, below-threshold wind stress concurred with a westward flow associated with relatively warm water entering into the GT, which was confined to the continental shelf (~50 km offshore), in the shelf break (from ~50 to ~100 km offshore) the SST decreased and the westward flow was less evident. Unfortunately, the HFRs were barely capable of recording the surface currents beyond 100 km offshore. Nevertheless, three pulses of relatively warm water coinciding with three of the longest periods with no wind (i.e., around 6 and 23 February, and 17 March) were registered approximately 200 km offshore (~14.5°N).

The geostrophic flow (relative to 200 dbar) associated with the thermohaline structure recorded by the CTD casts also revealed a shelf-limited westward coastal flow traveling alongshore, with opposite flow (eastward)

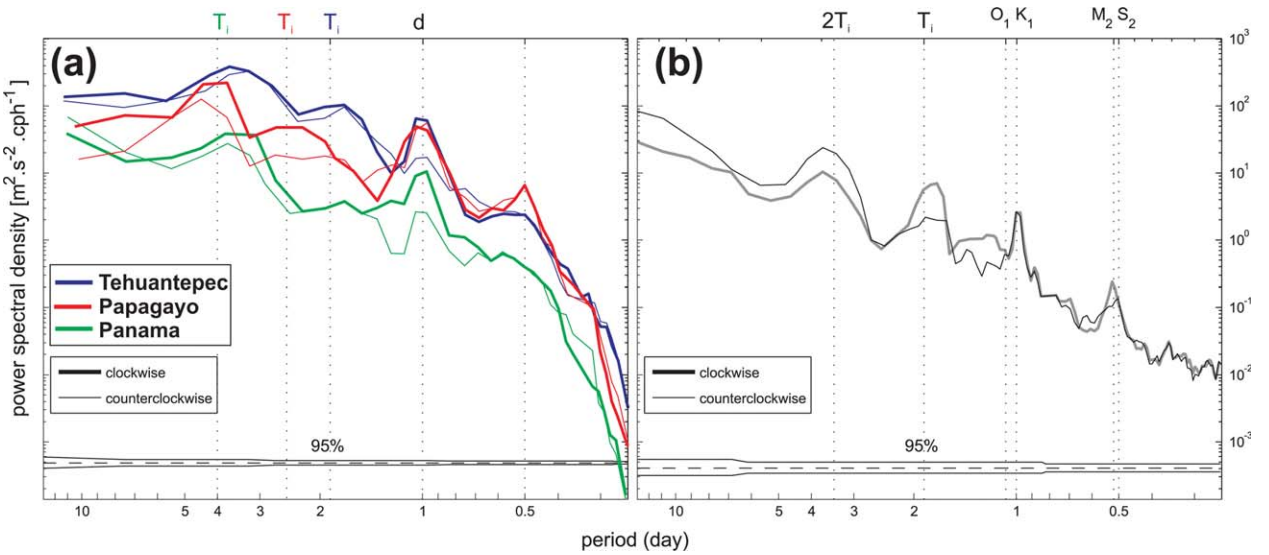

Figure 2. Power rotational spectra for (a) winds in the Gulf of Tehuantepec (blue line), Papagayo (red line), and Panama (green line); (b) sea surface currents measured by HFR. The 95% confidence limit is plotted in each panel.

farther offshore (~14.5°N, ~200 km offshore) (Figure 4a). The subinertial mean flow measured by HFR over a period of 2 months was in good agreement with the westward flow estimated by the geostrophic analysis (Figure 4b).

The observed coastal flow was surface-intensified within the first 100 m of the water column (Figure 5) and was associated with less saline (32) and warmer (30°C) waters flowing into the GT from the eastern region (Figure 5a). The salinity of this alongshore flow increased about 1.5 units at the center of the GT (Figure 5b). Further west, the flow became difficult to discern in the salinity records, but it was still clearly perceivable in

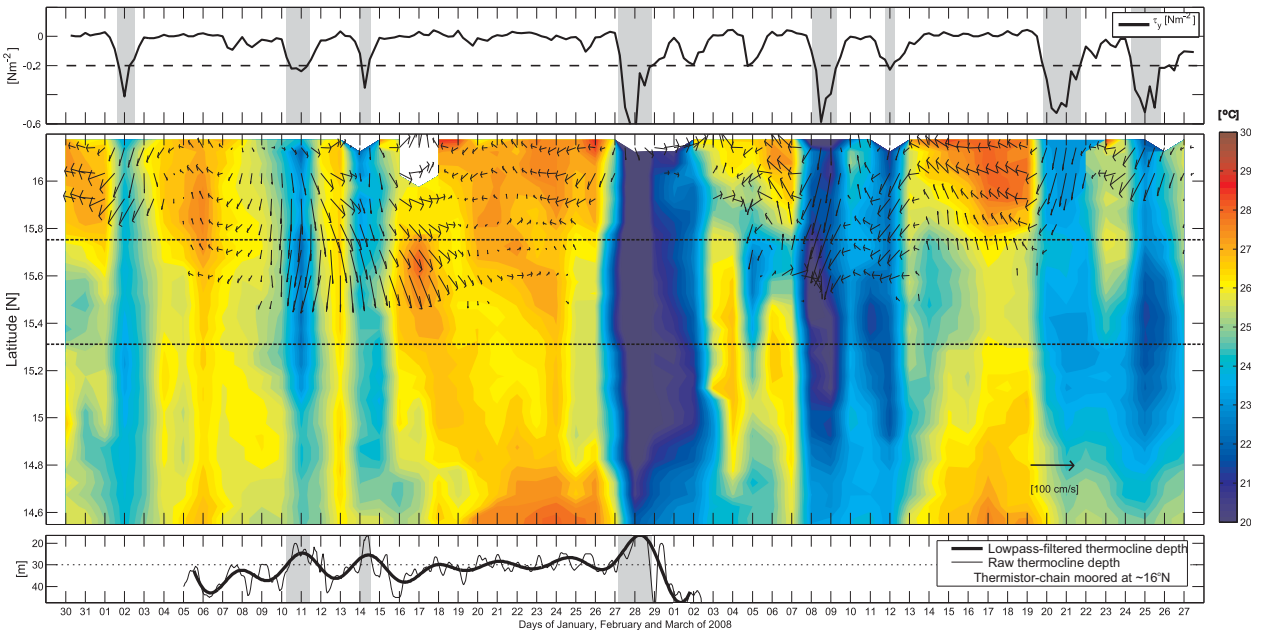

Figure 3. Sea surface currents (arrow vectors) along one cross-shore transect (red line in Figure 1) measured by HFR and sea surface temperature (color contours) from high-resolution satellite products. The top plot shows the offshore (negative) wind stress. Gray shades indicate gap wind events that exceed the threshold value of 0.2 Nm^{-2} [*Flores-Vidal et al.*, 2011]. The bottom plot shows the thermocline depth $\frac{dT}{dz} > 0.5\ ^{\circ}cm^{-1}$, where T is temperature in °C and dz is expressed in meters. The dashed lines at ~15.75°N and 15.3°N indicate the 100 and 1000 m isobaths, respectively, (i.e., the shelf break).

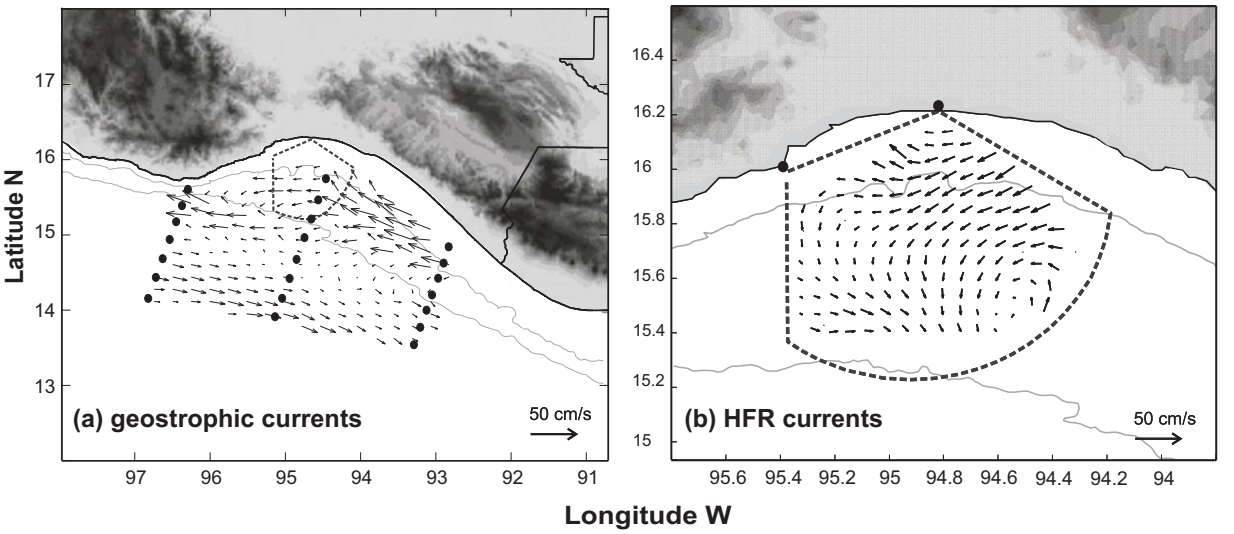

Figure 4. (a) Geostrophic current field estimated during a 5 day CTD cruise. Cast positions are indicated by bold dots. (b) Subinertial mean flow estimated from a 60 day time series measured by HFR. The dashed line polygon indicates ideal radar coverage. The two bold dots at the shore represent the HFR sites.

temperature records and geostrophic speed (Figure 5c). The relatively low salinity signature of this alongshore flow suggests that it may have its origin near the tropics, where it experiences important fresh water inputs from rain and river discharges [*Fiedler and Lavín*, 2006].

The temporal evolution of currents and temperature in the water column, as inferred from ADCP and thermistor-chain data respectively, is shown in Figure 6. Important wind events were identified on 10, 14, and 27 February. During these events, the cross-shore horizontal currents resembled a two-layer structure, with offshore currents above the thermocline and onshore currents below it (Figure 6b), while the vertical distribution of temperature (Figure 6c) suggests that wind jets did not disturb the subinertial periodicity of the thermocline oscillations (Figures 3, 6b, and 6c).

To corroborate the vertical structure of the subinertial variability, a power spectral density analysis of the nonfiltered thermistor-chain data as a function of depth and period was made. The most energetic signal with a period of ~4 days occurred at a depth of ~30 m, which corresponded to the thermocline oscillations (Figure 7a), while currents near the same depth oscillated clockwise with the same periodicity of ~4 days (Figure 7b). Therefore, Figure 7 shows that thermocline and current oscillations, with periodicity of ~4 days, were persistent throughout the entire studied period.

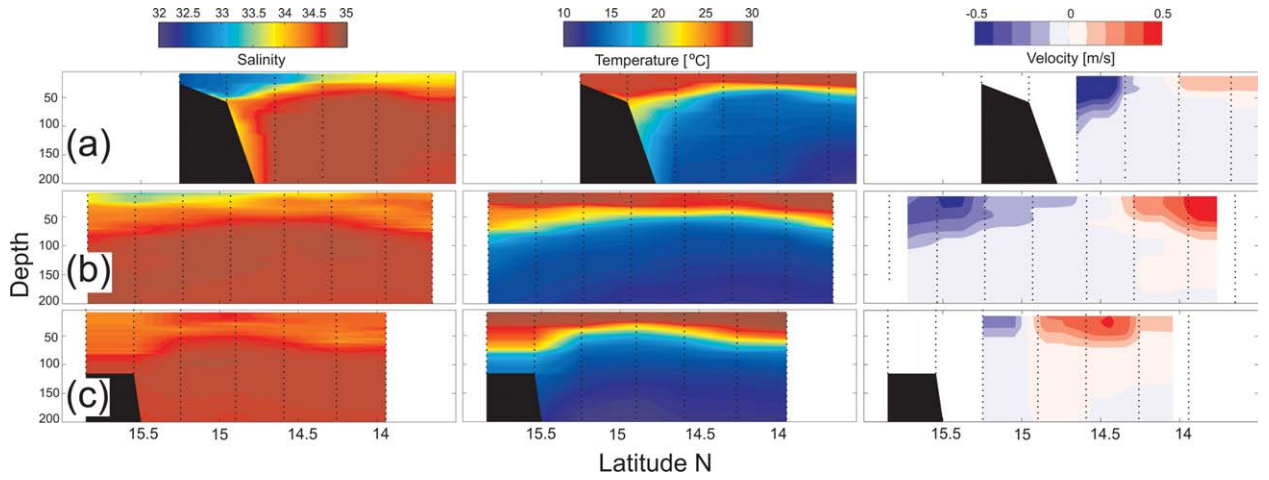

Figure 5. (left) Vertical distribution of salinity, (middle) temperature, and (right) geostrophic speed from the surface to 200 m depth. Cross-shore transect at (a) ~93°W (eastern Gulf), (b) ~95°W (Gulf's main axis), and (c) ~97°W (western Gulf).

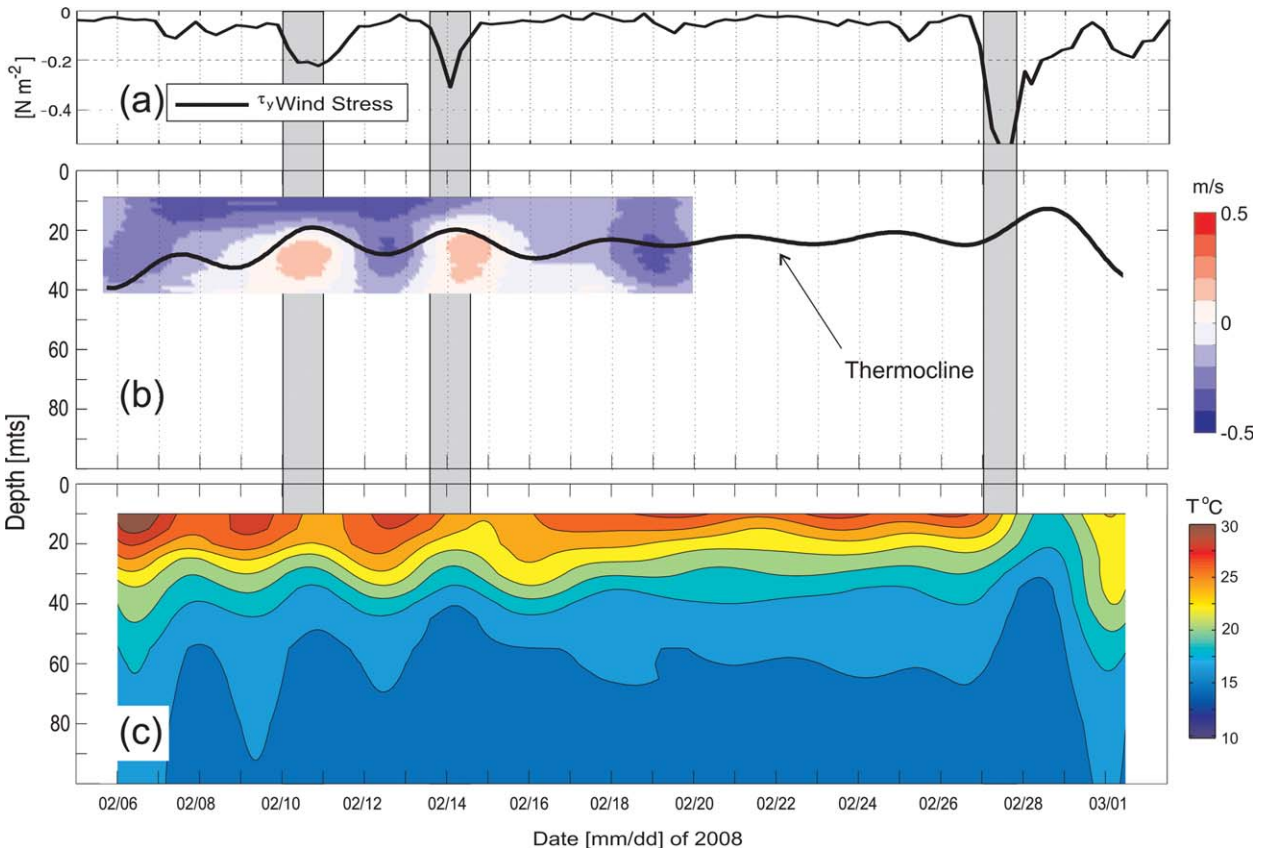

Figure 6. Temporal evolution of (a) the cross-shore component of the wind stress, (b) the vertical distribution of the cross-shore subinertial currents, and (c) the vertical distribution of the temperature. Shaded areas represent wind jet events. The mooring position is shown in Figure 1.

To further study these 4 day oscillations, a band-pass filter with a window centered on 3–5 days was applied to the HFR data. The band-passed signal was used to calculate empirical orthogonal functions (EOF). The first temporal mode, explaining approximately 60% of the variability, was in good agreement with the vertical displacements of the thermocline (Figure 8a). The divergence contours and arrow vectors from the band-pass signal (Figure 8b) show that the 4 day oscillations were intensified at the shore and were permanent features regardless the wind jet. Figure 9 shows the spatial and temporal modes obtained from the EOF analysis. Mode 1 resembled an alongshore current both temporally and spatially. It intensified at the shore and changed its sign every 2 days (4 day oscillation). Spatial mode 2 behaved more like a cyclonic eddy centered on the shelf break, and although it explained only 18% of the band-pass signal, its temporal component was very similar to mode 1.

A physical mechanism that may explain these EOF results is a CTW, which requires the wind as forcing mechanism. The wind jets over the GPP and the GPN are the main mechanisms inducing strong enough perturbations capable of traveling along the coast from low to high latitudes into eastern tropical Pacific. In order to examine which of the two regions was directly related to the 4 day oscillations at the GT, coherence analyses were made [*Gonella*, 1972; *Fofonoff*, 1969] between alongshore and cross-shore winds at the GT, GPP, and GPN, and the alongshore and cross-shore currents (as measured by HFR), SST (from satellite products), and thermocline depth (Figure 10). All coherence analyses were made before applying low-pass or band-pass filters to the time series.

Alongshore local (GT) winds did not show any spectral coherence with alongshore currents (Figure 10a), cross-shore currents (Figure 10b), SST (Figure 10c), or thermocline depth (Figure 10d). This suggests that most of the subinertial variability of the alongshore currents in the GT was not locally wind driven. By contrast, cross-shore local winds showed significant coherence around the local (GT) inertial period with cross-

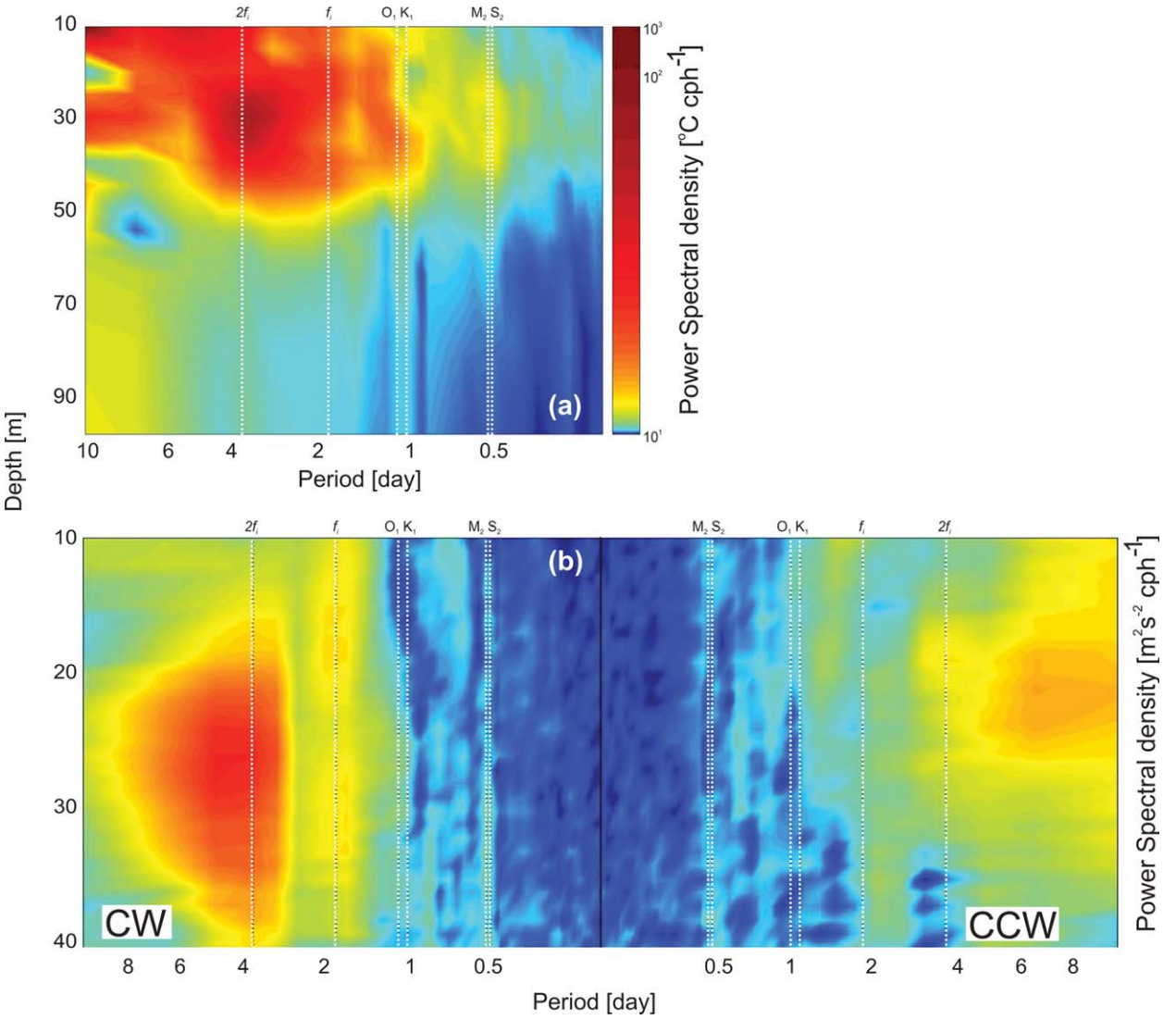

Figure 7. Power spectral density as a function of period and depth for (a) temperature and (b) currents.

shore currents (Figure 10f) and thermocline depth (Figure 10h), as expected due to the strong offshore wind outburst. Remote forcing was evidenced by the significant spectral coherence between alongshore local (GT) currents and remote (GPP) alongshore winds (Figure 10a) and the remote (GPN) cross-shore winds (Figure 10e). The local (GT) thermocline depth was significantly more coherent with both cross-shore and alongshore GPN winds (Figures 10d and 10h). The local SST showed significant coherence with alongshore GPP winds (Figure 10c). Interestingly, most peaks of significant coherence were found near the corresponding inertial frequencies for the GPP and the GPN ($f \approx 0.4$ and 0.25 cpd, respectively).

Since the local GT wind jets modified the thermocline and the cross-shore currents by means of inertial oscillations (Figures 10f and 10h), this dynamic scheme may also hold for the GPP and the GPN. At these remote locations, wind jets may have induced the same variability into the ocean but with the signature of their local inertial frequencies ($f \approx 0.4$ and 0.25 cpd, respectively). These oscillations may have traveled poleward trapped by the shelf with the coast on the right-hand side, as detected for the HF radio scatterometers deployed at the GT.

The results of a lag-correlation analysis between the alongshore and cross-shore winds of the GT, GPP, and GPN and the local (GT) thermocline depth are shown in Table 1. The lag between the local (GT) wind and the vertical displacement of the local thermocline was about 6–24 h, showing the rapid response of the

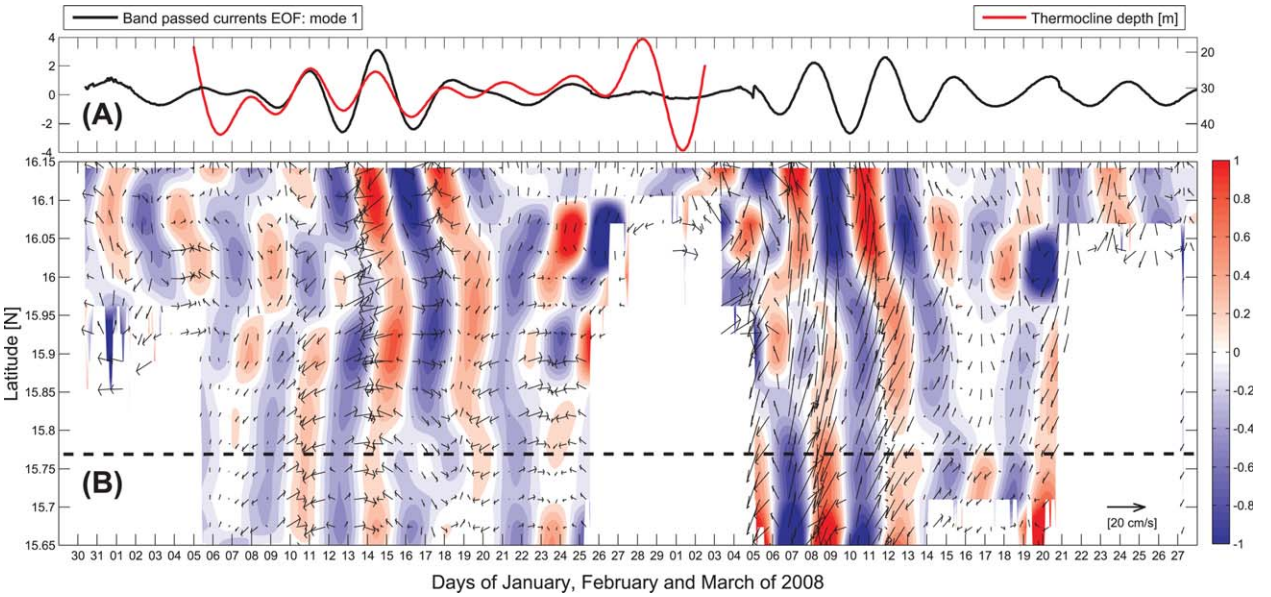

Figure 8. (a) Temporal mode 1 (black line) from the EOF analysis after applying a band-pass filter and thermocline depth (red line). (b) Normalized divergence (blue and red contours) of the band-pass filtered HFR currents extracted from the same transect as in Figure 3. The dashed line shows the shelf (100 m isobath).

system to the local wind jet. By contrast, lags of ∼720–756 h (∼30 days) and 1440–1488 h (∼60 days) were computed between the local thermocline and the remote GPP and GPN winds, respectively. Along with the coherence analysis, these lag-correlations suggest the presence of CTWs that may have been generated at the GPN and the GPP. The basic properties of these CTWs, such as frequency ω, wave number k, and phase speed c, are discussed at the end of the next section by means of baroclinic and barotropic numerical models.

4. Discussion

The classic circulation scheme of the eastern tropical Pacific ocean described by *Wyrtki* [1965] and *Kessler* [2002], in particular the coastal current off the Mexican southwest coast and its direct relation with the Costa Rica Coastal Current (CRCC), has hitherto been difficult to reconstruct [*Trasviña and Barton*, 2008; *Barton et al*., 2009]. Using numerical simulations, *Zamudio et al*. [2006] report a poleward traveling shelf break front (SBF) in the southwest of Mexico. Although their numerical simulations do not include the coastal shelf area (<50 km offshore), the authors relate this SBF to CTWs generated in the equatorial Pacific rather than to the CRCC. In a subsequent study, *Zamudio et al*. [2008] show numerically simulated evidence of CTWs traveling poleward as far as the GT; however, these CTWs originate in the GPN and not at the equator, as originally reported. Using CTD data obtained during two oceanographic cruises in the GT, *Barton et al*. [2009] report a westward coastal flow similar to the one reported by *Zamudio et al*. [2006]. The authors describe the water mass as warm and low salinity waters coming from Central America.

In the present work, we studied the subinertial dynamics of the GT. One poleward traveling SBF was identified based on salinity, temperature, and geostrophic fields. This SBF was evidenced by the intrusion of less saline and relatively warm waters into the GT. The flow was confined to the coast (<50 km offshore), with thermocline doming at the shelf break (∼60 km offshore). On the other hand, thermistor-chain data revealed vertical thermocline oscillations with a period of 4 days, which were in spectral coherence with the alongshore surface currents measured with HFR scatterometers. Band-pass filtered currents and EOF analyses showed that the 4 day oscillations were a persistent feature that may be explained as CTW. Spectral coherence analyses and lag correlations revealed significant coherence between the GPN winds and the local (GT) subinertial currents (Figure 10 and Table 1). This suggests that the proposed CTW may have originated further south. In the following section, we present the results of baroclinic and barotropic numerical CTW models to verify if the observed subinertial oscillations are in good agreement with basic properties of CTW.

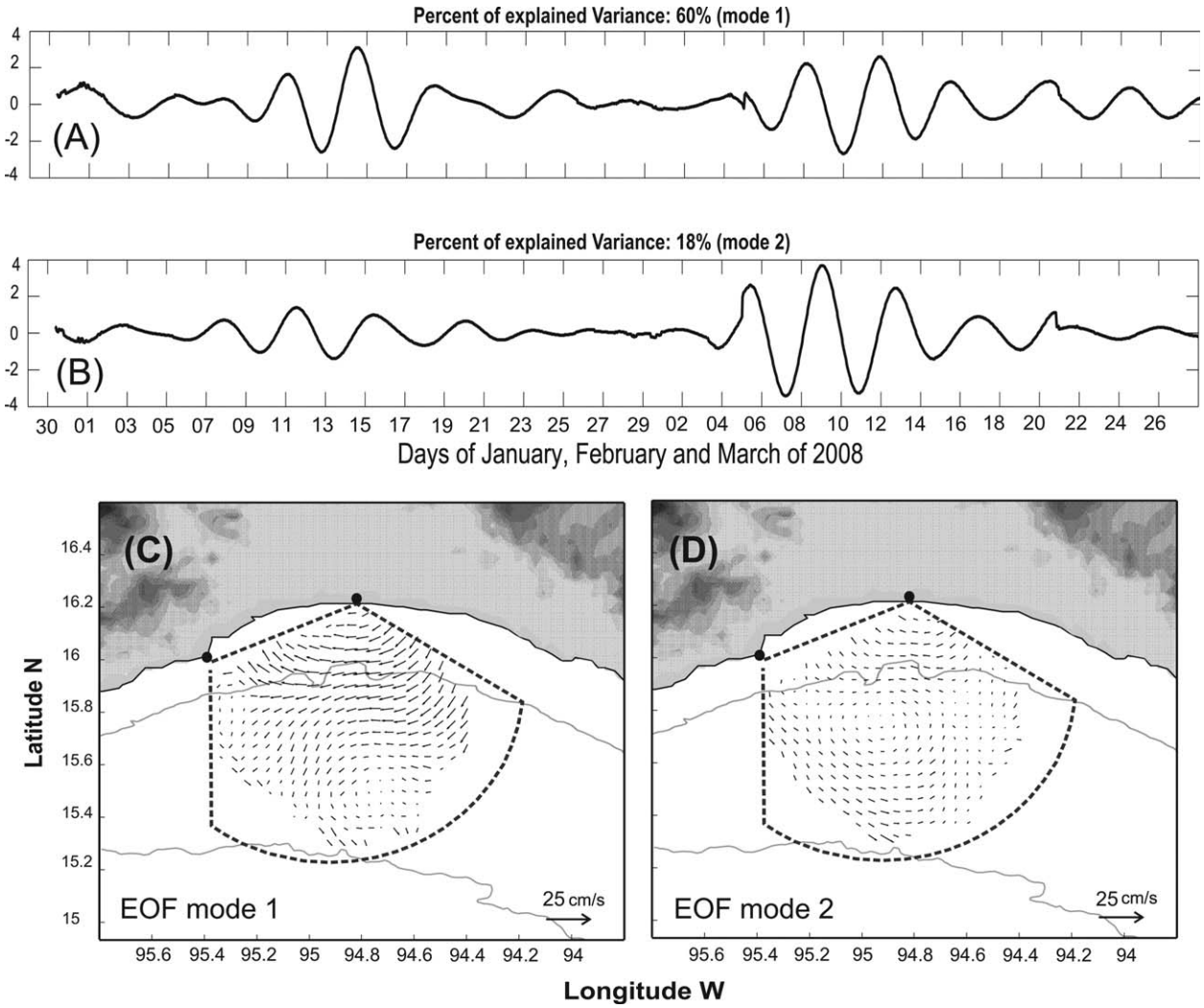

Figure 9. Spatial and temporal modes obtained from the EOF analysis after applying a band-pass filter to the HFR surface currents. (a and b) The temporal modes 1 and 2, which explain 60% and 18% of the variability; (c and d) the corresponding spatial modes.

4.1. Models of Coastal-Trapped Waves

The observations detailed above suggest that oscillations with near-inertial frequencies were generated in the GPP and the GPN and that these perturbations traveled northward, manifesting at the GT as subinertial oscillations with a period of approximately 4 days. In order to discuss whether the observed motions match CTW properties, we explored some simplified models of coastal topographic waves. We applied the baroclinic and barotropic numerical model written by *Brink and Chapman* [1987] (hereafter referred to as BC models), which search for resonant frequencies ω, associated with wave number k, using an iterative process over an arbitrary coastal topography.

The application of the BC models requires the shape of the bottom topography in the region of interest. Figure 11a shows the average offshore profile along ~100 km between the GPN and the GT, with a superimposed depth profile $h(x)$ written as an arbitrary power of the offshore coordinate x

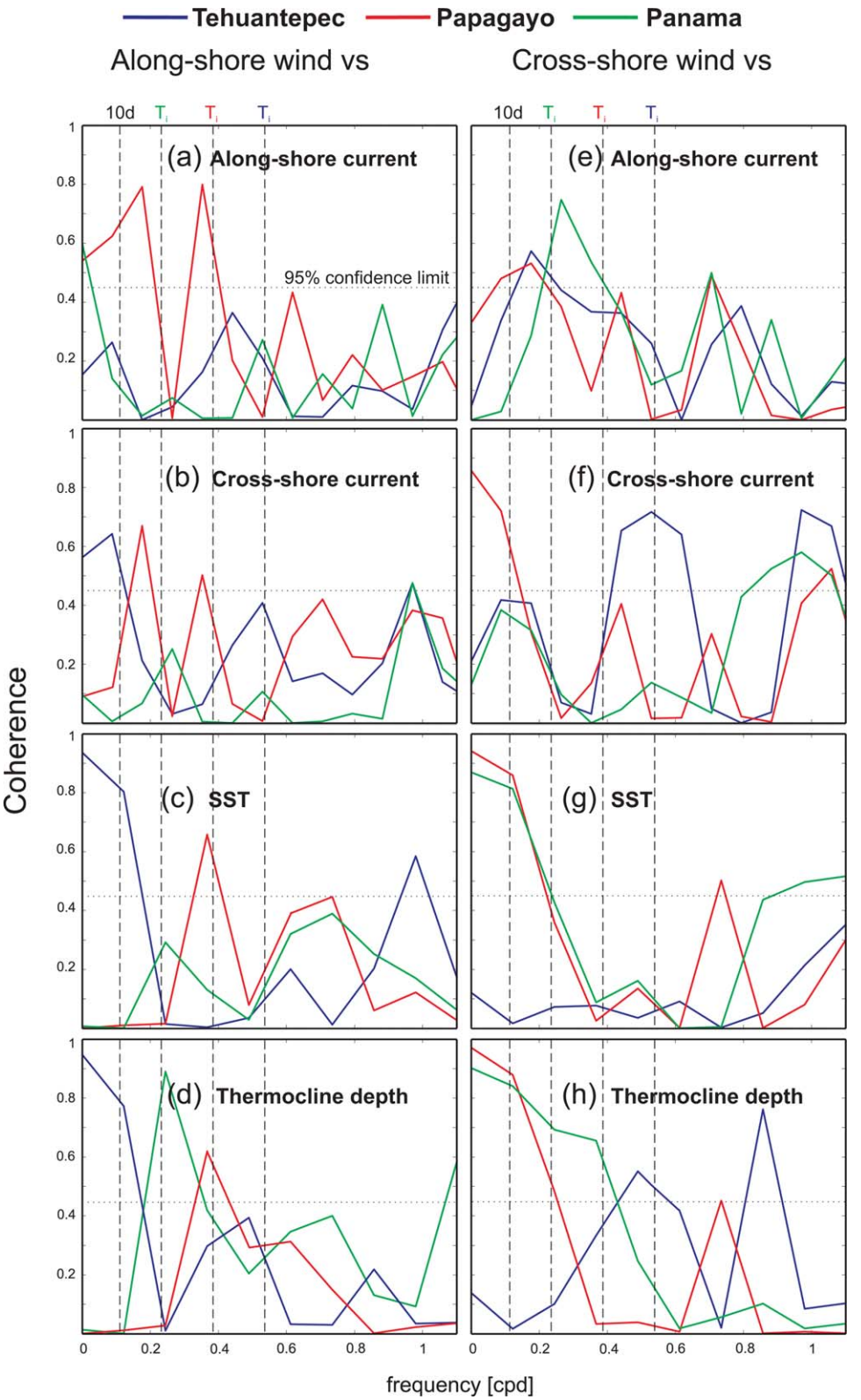

Figure 10. Spectral coherence analysis. (a–d, left column) alongshore winds in the Gulf of Tehuantepec (blue line), Papagayo (red line), and Panama (green line) versus (a) alongshore currents, (b) cross-shore currents, (c) satellite sea surface temperature, and (d) thermocline depth. (e–h, right column) cross-shore winds in the Gulf of Tehuantepec (blue line), Papagayo (red line), and Panama (green line) versus the same variables as Figures 10a–10d. The inertial period of each location is indicated by the vertical dashed lines. The 95% confidence intervals are indicated by the horizontal dotted line.

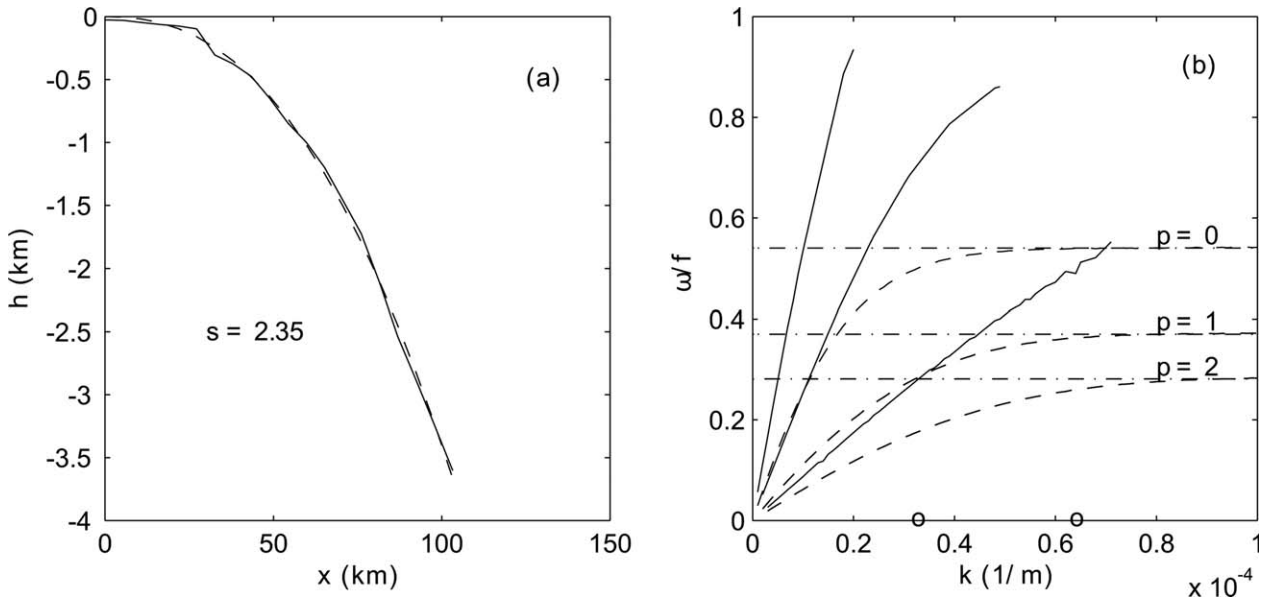

Figure 11. (a) Solid line: average profile of the offshore bottom topography between the Gulf of Papagayo and the Gulf of Tehuantepec, as calculated from a set of 10 cross-shore profiles, each one with a length of approximately 100 km, obtained from ETOPO2 data (available at http://www.ngdc.noaa.gov/mgg/global/etopo2.html). Dashed line: profile $h = h_o(\lambda x)^s$ with topographic parameters $h_o = 990$ m, $\lambda^{-1} = 59$ km, and $s = 2.35$. (b) Solid lines: numerically calculated baroclinic dispersion curves for the first three modes. Dashed lines: corresponding barotropic dispersion curves. Dashed-dotted lines: barotropic frequency limits calculated with equation (3). Circles indicate the wave number k of oscillations with a wavelength of 200 and 100 km.

$$h(x) = h_o(\lambda x)^s, \tag{1}$$

where the parameter $s > 0$ represents the shape of the shelf, and h_o and λ^{-1} are the vertical and horizontal scales, respectively. Fitting this expression to the average profile resulted in a fair representation of the coastal topography and was therefore used in the numerical codes.

For the baroclinic analysis, we used an exponential N^2 vertical profile [*Brink*, 1982; *Dale et al*., 2001]

$$N^2 = N_o^2 \exp(-z/z_o), \tag{2}$$

with $N_o^2 = 2.2 \times 10^{-3} s^{-2}$ and $z_o = 100$ m, which is an acceptable approximation of typical profiles in the study area during winter [*Emery et al*., 1984].

The numerically calculated baroclinic and barotropic dispersion relations are shown in Figure 11b (for details of the numerical parameters we refer to *Zavala-Sansón* [2012]). The $\omega - k$ relationship was approximately linear for long waves (small k). The frequencies of the first two baroclinic modes rapidly approached the inertial value, which is in agreement with the observations that suggested the generation of nearly inertial waves in the GPP and the GPN. Since the numerical method did not allow super inertial frequencies, dispersion curves were truncated as they approached the inertial value. The pronounced tendency toward near-inertial frequencies was observed for different N^2 profile types (results not shown).

Table 1. Cross-Correlation Between the Along- and Cross-Shore Winds of the Gulf of Tehuantepec (GT), Gulf of Papagayo (GPP), and Gulf of Panama (GPN) and the Thermocline Depth in the GT

	Alongshore Wind		Cross-Shore Wind	
	Lag (h)	R^2	Lag (h)	R^2
GT	24	−0.75	6	0.83
GPP	756	0.65	720	0.71
GPN	1488	0.7	1440	0.65

According to the lag correlation analysis, the time for a signal to travel from the GPP (GPN) to the GT (i.e., 1000 (1800) km) was approximately 30 (60) days (Table 1), which corresponds to a phase speed of $c \approx 30$ km d^{-1}. For the second baroclinic mode, a 200 km long wave was nearly inertial ($\omega/f \approx 0.8$) with phase speed of $c \approx 38$ km d^{-1}, which is slightly higher than the expected value. The third baroclinic mode behaved slightly different, a 100 km long wave had lower phase speed of $c \approx 27$ km d^{-1} which agrees better with the lag analysis.

However, the frequency of this wave was lower ($\omega/f \approx 0.5$).

For completeness, the barotropic dispersion curves are also presented (Figure 11b). The $\omega - k$ relationship was also approximately linear for long waves, but with a less steep slope than the baroclinic case. For the first barotropic mode, a 100 km long wave had phase speed of c $\approx$ 28 km d^{-1}, which was close to the expected value. The barotropic frequencies had an upper limit; therefore, they were clearly subinertial. The upper limit values can be calculated analytically for waves over the infinite family of x^s-bottom profiles as

$$\frac{\omega}{f} = \frac{s}{2(p+1)+s}, \tag{3}$$

with $p \geq 0$ being a positive integer indicating the wave mode [*Zavala-Sansón*, 2012].

Taken together, the baroclinic model supports the idea of a nearly inertial wave in a stratified environment, that is, a baroclinic wave generated in the GPP or the GPN traveling along the coast to the GT. In addition, the barotropic calculations suggest that the expected phase speed corresponds well to that of a subinertial topographic wave in the GT. These results provide plausible evidence for the transition from a nearly inertial wave at one location (southern) to a subinertial wave at other location (northern). However, definite conclusions cannot be drawn on the basis of these models because of several inherent limitations. Among others, the models do not allow changes in the Coriolis parameter (f) and must be applied to the same cross-shore topography. Moreover, the baroclinic calculations tend to fail as the wave frequencies approach inertial values. To our knowledge, this problem has not been addressed in the literature and would need to be treated in a separate paper.

5. Conclusions

In the present work, we provide evidence for the presence of CTWs along the southwestern coast of Mexico. The CTWs are generated at low latitudes (GPN, ~7°N) and travel about 1800 km to the GT (~16°N). The mechanism triggering these CTWs may be a negative sea level anomaly generated by the inertial component of the strong offshore wind jets, either in the GPN or the GPP. Once developed, CTWs propagate toward the north along the shelf break that acts as a topographic wave guide. Lag correlation analyses showed travel times of ~30 (60) days from the GPP (GPN) to the GT, corresponding to a phase speed of approximately 30 km d^{-1} (~30 cm s^{-1}).

According to the CTW models, there is a wave signal traveling from the GPP and the GPN to the GT with a phase speed in good agreement with our observations. Baroclinic modes suggest that CTWs are generated at near-inertial frequencies of the studied locations, while barotropic modes suggest that the CTWs could become subinertial further north of its generation site. Finally, if CTWs are generated somewhere near the GPN, and are later detected in the GT, CTWs may also be generated locally in the GT by the same mechanism (i.e., inertial component of the wind jet), and could be later detected at northern latitudes (>16°N). Although there are some numerical studies that suggest the presence of CTWs near the north bound of the eastern tropical Pacific (i.e., latitudes of ~20°N) [*Zamudio et al.*, 2008], to our knowledge there are no measurements that show the presence of CTWs further north than the GT, caused by the inertial component of the wind outburst over the GT.

Acknowledgments

Xavier Flores-Vidal was funded by the CONACyT (Mexican Council of Science) PhD scholarship from 2006 to 2010, and a supplementary international work stay stipend in 2007. The Mexican Navy Ministry SEMAR and its oceanographic research station at Salina Cruz, Oaxaca, were of great help during the HFR field deployments. Funding for field experiments was provided by CONACyT research projects U40822-F, 85108, and 155793. Programs 323, 341, and 361 of the Autonomous University of Baja California provided additional funding. Pierre Flament and Cedric Chavanne were funded by the State of Hawaii and by the National Science Foundation (grants OCE-9724464, -9819534, -0426112, and -0453848). K. H. Brink kindly shared the CTW models that were used in this work. We sincerely thank Andrew Dale and anonymous reviewers who improved this work with their helpful suggestions.

References

Allen, J. S. (1975), Coastal trapped waves in a stratified ocean, *J. Phys. Oceanogr.*, *5*, 300–325.

Barrick, D. E., M. W. Evans, and B. L. Weber (1977), Remote sensing of the troposphere, *Science*, *198*, 138.

Barton, E. D., M. Lavin, and A. Trasviña (2009), Near-shore circulation of the Gulf of Tehuantepec under offshore wind, *Cont. Shelf Res. 29*, 485–500.

Blackburn, M. (1962), An oceanography study of the Gulf of Tehuantepec, *Fish Wildl. Serv. Spec. Sci. Rep. Fish.*, *404*, 28 p.

Brandhors, W. (1958), Thermocline topography, zooplankton standing crop, and mechanisms of fertilization in the eastern tropical Pacific, *J. Cons. Int. Explor. Mer.*, *24*, 16–31.

Brink, K. H. (1982), A comparison of long coastal trapped wave theory with observations off Peru. *J. Phys. Oceanogr.*, *12*, 897–913.

Brink, K. H. (1991), Coastal-trapped waves and wind-driven currents over the continental shelf, *Annu. Rev. Fluid Mech.*, *23*, 389–412.

Brink, K. H., and D. C. Chapman (1987), Programs for computing properties of coastal-trapped waves and wind-driven motions over the continental shelf and slope, *Tech. Rep. WHOI-87-24*, 2nd ed., pp. 119, Woods Hole Oceanogr. Inst., Woods Hole, Mass.

Christensen, N., R. De la Paz, and G. Gutierrez (1983), A study of sub-inertial waves off the west coast of Mexico, *Deep Sea Res., Part A*, *30*, 835–850.
Clarke, A. J. (1977), Observational and numerical evidence for wind-forced coastal trapped long waves, *J. Phys. Oceanogr.*, *7*, 231–247.
Csanady, G. T. (1977), The arrested topographic wave, *J. Phys. Oceanogr.*, *6*, 47–62.
Dale, A. C., J. M. Huthnance, and T. J. Sherwin (2001), Coastal trapped-waves and tides at near-inertial frequencies, *J. Phys. Oceanogr.*, *31*, 2958–2970.
Emery, W. J., W. G. Lee, and L. Magaard (1984), Geographic and seasonal distributions of BruntVisl frequency and Rossby radii in the North Pacific and North Atlantic, *J. Phys. Oceanogr.*, *14*, 294–317.
Enfield, D. B., and J. S. Allen (1983), The generation and propagation of sea level variability along the Pacific coast of Mexico, *J. Phys. Oceanogr.*, *13*, 1012–1033.
Fiedler, P. C., and M. Lavin (2006), A review of eastern tropical Pacific oceanography, *Prog. Oceanogr.*, *69*, 2–4.
Flores-Vidal, X., C. Chavanne, R. Durazo, and P. Flament (2011), Coastal circulation under low wind conditions in the Gulf of Tehuantepec, Mexico: High frequency radar observations, *Cienc. Mar.*, *37*(4A), 493–512.
Flores-Vidal, X., P. Flament, R. Durazo, C. Chavanne, and K. W. Gurgel (2013), High-frequency radars: Beamforming calibrations using ships as reflectors, *J. Atmos. Oceanic Technol.*, *30*(3), 638–648, doi:10.1175/JTECH-D-12-00105.
Fofonoff, N. (1969), Spectral characteristics of internal waves in the ocean, *Deep Sea Res. Oceanogr. Abstr.*, *16*, 58–61.
Gill, A. E., and A. J. Clarke (1974), Wind-induced upwelling, coastal currents, and sea-level changes, *Deep Sea Res. Oceanogr. Abstr.*, *21*, 325–245.
Gonella, J. (1972), A rotary-component method for analysing meteorological and oceanographic vector time series, *Deep Sea Res., Oceanogr. Abstr.*, *19*, 833–846.
Gurgel, K., G. Antonischki, H. Enssen, and T. Schlick (1999), Wellen radar wera: A new ground-wave HF radar for ocean remote sensing, *Coastal Eng.*, *37*, 219–234.
Huthnance, J. M. (1978), On coastal trapped waves: Analysis and numerical calculation by inverse iteration, *J. Phys. Oceanogr.*, *8*, 74–92.
Kessler, W. (2002), Mean three-dimensional circulation in the northeast tropical pacific, *J. Phys. Oceanogr.*, *32*, 2457–2471.
Merrifield, M. (1992), A comparison of long coastal-trapped wave theory with remote-storm-generated wave events in the Gulf of California, *J. Phys. Oceanogr.*, *22*, 5–18.
Mysak, L. A. (1968), Edgewaves on a gently sloping continental shelf of finite width, *J. Mar. Res.*, *26*, 24–33.
Romero-Centeno, R., J. Zavala, A. Gallegos, and J. Obrien (2003), Isthmus of Tehuantepec wind climatology and ENSO signal, *J. Clim.*, *16*, 2628–2639.
Zavala-Sansón, L. (2012), Simple models of coastal-trapped waves based on the shape of the bottom topography, *J. Phys. Oceanogr.*, *42*, 420–429, doi:10.1175/JPO-D-11–053.1.
Steenburgh, W., D. M. Schultz, and B. A. Colle (1998), The structure and evolution of gap outflow over the Gulf of Tehuantepec, México, *Mon. Weather Rev., 126*, 2673–2691.
Trasviña, A., and E. D. Barton (2008), Summer mesoscale circulation in the Mexican tropical Pacific, *Deep Sea Res., Part I*, *55*, 587–607.
Wyrtki, K. (1965), Surface currents of the eastern tropical Pacific Ocean, *Inter Am. Trop. Tuna Comm. Bull.*, *9*, 271–304.
Zamudio, L., P. Leonardi, S. Meyers, and J. O'Brien (2001), ENSO and eddies on the southwest coast of México, *Geophys. Res. Lett.*, *28*(1), 13–16, doi:10.1029/2000GL011814.
Zamudio, L., H. Hurlburt, E. Metzger, S. Morey, J. O'brien, C. Tilburg, and J. Zavala (2006), Interannual variability of the Tehuantepec eddies, *J. Geophys. Res.*, *111*, C05001, doi:10.1029/2005JC003182.
Zamudio, L., E. Metzger, and P. J. Hogan (2008), A note on coastally trapped waves generated by the wind at the Northern Bight of Panamá, *Atmósfera*, *21*(3), 241–248.